Inner UV Taper Weighting for Synthesis Imaging

W. D. Cotton, August 14, 2017

***Abstract*—The use of a Gaussian taper to downweight the shorter ("inner") baselines of a synthesis array is described. The technique is applied to MeerKAT 16 antenna data. More distant sidelobes are reduced as expected but this did not produce the expected increase in dynamic range. The dynamic range in this MeerKAT data appears to be uv coverage limited.**

***Index Terms*—imaging, interferometry**

I. Introduction

SYNTHESIS imaging allows flexibility in shaping the synthesized beam. Weighting in uv space can be used to enhance the desired qualities of the data, e.g. resolution or surface brightness or reduce undesirable features such as sidelobes. UV weighting can be used to augment the properties of an interferometer layout.

General purpose interferometers with static element locations (e.g. MeerKAT, ngVLA, SKA) have the problem that they must cover a range of science cases leading to designs that are suboptimal for any application. New or enhanced uv weighting schemes may be needed to make the best use of these instruments. This memo considers the case of the incomplete MeerKAT array with 16 antennas. MeerKAT is optimized for pulsar and HI observations so is very centrally condensed but has baselines to 8 km to facilitate some continuum imaging. Uniform or Briggs weighting helps in this case by downweighting the regions of uv space with higher densities of observations. This comes at a cost of reduced sensitivity but produces a synthesized beam which is much better for extra-galactic continuum observations.

In the following the technique of "inner uv tapering" is considered to augment Briggs weighting. Tapering is generally used to reduce the weight of longer baselines to reduce the resolution and enhance surface brightness sensitivity. A similar technique can be applied in conjunction with Briggs weighting to the inner regions of the uv plane to reduce the sidelobes of the synthesized beam. This memo evaluates this technique using the Obit package [1] [1].

II. Sidelobes and Sensitive Observations

To help motivate this discussion, consider the effects of sidelobes on sensitive data approaching the "confusion" limit at which there are multiple weak sources contributing to each resolution element. If perfect deconvolution were possible, there would not be a problem and artifacts due to these sidelobes would be fully removed. In practice, deconvolution is always less than perfect in the sense that the assumed beam shape differs from the true beam shape. This can be the result of a number of effects especially imperfect calibration and pointing errors. Imperfect beam deconvolution will limit the dynamic range in the image by scattering power from sources across the field. Emission below the level of the "crud" will not be reliably detected no matter what the "thermal" noise level is.

III. UV Weighting

In synthesis imaging a weight can be assigned to each datum to control the properties of the derived image. If the weights are proportional to sensitivity ("Natural weighting"), the derived image will have the maximum sensitivity. On the other hand, the maximum sensitivity image may have undesirable properties. For centrally condensed arrays (as most are) the resolution will be lower than given by the longest spacings. "Uniform" weighting is giving uv cells the same weight rather than visibilities and will result in a point spread function (psf) with a sharper central peak and lower sidelobes. "Briggs" weighting allows weighting between these two extremes.

If lower surface brightness emission is desired than is well detected in a uniform weighted image, tapering, multiplying the longer spacing's weight by a Gaussian function decreasing to longer baselines can be used to reduce the resolution while increasing the surface brightness sensitivity.

IV. Very Centrally Concentrated Arrays

Reconfigurable arrays such as WSRT, VLA, ATCA can have configurations designed for various purposes. Stationary arrays such as MeerKAT, ngVLA and SKA while they may contain many antennas, only one configuration is available for all use cases. Thermal line observations need good surface brightness sensitivity (i.e. many short baselines) and pulsar searches are most easily done with large synthesized beams (again many short baselines). These considerations may drive array configurations to be very centrally condensed. In these cases, Uniform/Briggs/Tapering may not be adequate for use cases needing higher resolution and a well behaved psf.

Consider the case of MeerKAT in its current (August 2017) 16 antenna condition. This array is very centrally condensed. An azimuthally averaged rendition of the naturally weighted psf derived for a calibrator used in a full synthesis is shown in Figure 1. A uniform weighted image would have a psf of $\approx 6''$. The psf from the same data imaged with Briggs Robust weighting is shown in Figure 2. This psf has much lower sidelobes but there is a major sidelobe nearly $40''$ from the core. This sidelobe covers a substantial area in the image and incompletely corrected will corrupt the image much more than a comparable sidelobe closer to the center.

National Radio Astronomy Observatory, 520 Edgemont Rd., Charlottesville, VA, 22903 USA email: bcotton@nrao.edu

[1] http://www.cv.nrao.edu/∼bcotton/Obit.html

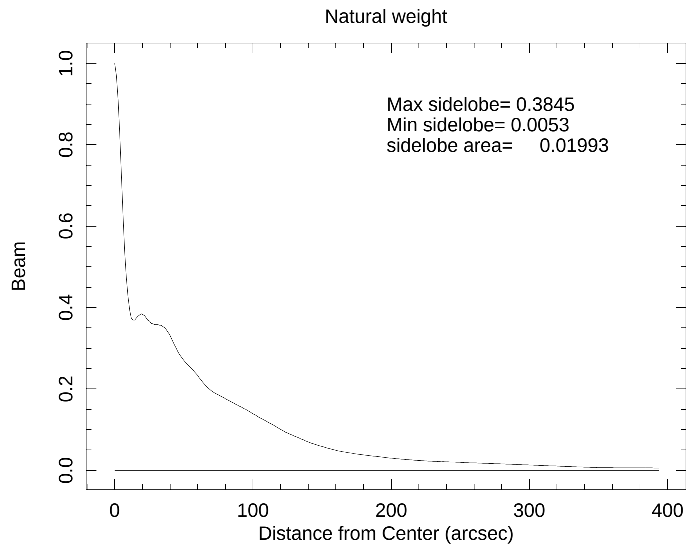

Fig. 1. The azimuthally averaged beam power for a naturally weighted calibrator observation with the 16 element MeerKAT array. The width of the central peak is 23″ FWHM while the psf still has power past 5’ and very significant power to 2’

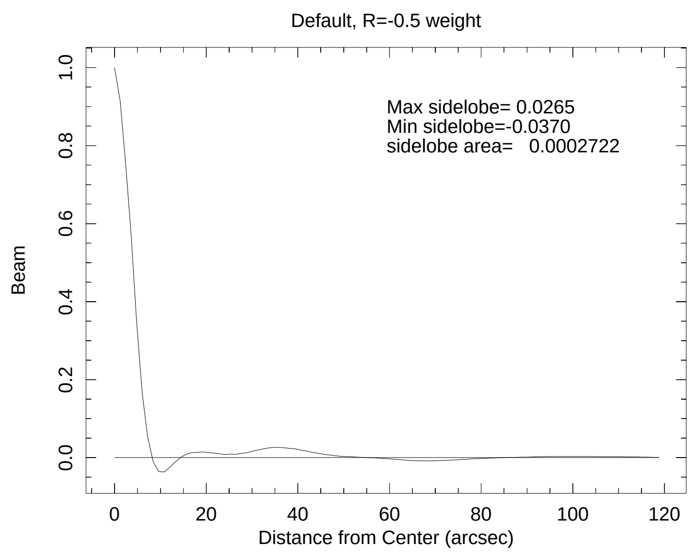

Fig. 2. Like Figure 1 but with Briggs Robust weighting -0.5 (AIPS,Obit usage) and only the inner portion. The FWHM is 7.4″ and with much lower sidelobes outside the inner 10”.

V. Inner UV Taper

Very short interferometer baselines are subject to various corrupting effects as RFI, shadowing and cross–talk and for observation not needing these spacings, they are frequently removed using an inner UV limit. Such a limit puts a sharp edge in the uv coverage which will produce ringing in the derived psf. As a softer way of cutting off the very shortest spacing and reducing the influence of the shorter baselines in general consider an “inner taper”:

$$weight \ = \ 1 \ - \ e^{-(u^2+v^2)/2\sigma_{inner}^2}$$

where u and v are the spatial frequency coordinates and σ_{inner}^2 is the variance of the inner Gaussian taper.

This was implemented in Obit in the ObitUVWeight class parameterized as an elliptical Gaussian, UVITaper, in which the sigmas are the spacing at which the weight is 0.7. This weight factor is multiplied times any other weighting applied to the data. The implementation is analogous to that of the outer taper.

VI. Evaluation

While the functional form of the inner tapering is simple, its effect on real data it difficult to predict as it depends on the details of the uv coverage. Thus, numerical evaluations were done imaging real data sets in the Obit wide-band, wide-field imager MFImage [2] upgraded to apply an inner taper. Imaging used a joint frequency deconvolution to accommodate the wide bandwidth of the data and faceting was used to cover the wide field of view. Facets were also placed around bright outlying sources from the SUMMS catalog.

The effectiveness of inner tapering was tested on a 16 antenna MeerKAT data set with a full track (12 hours) on a circumpolar field devoid of strong sources. There were two types of test, ones using the phase reference calibrator which were quick enough to run to test a range of parameters and tests on the target field to evaluate effects on imaging and the suitability for a confusion P(D) analysis.

A. Calibrator Beam

The phase reference calibrator, at a declination of 71° S, was observed for 8 sec. every 6 minutes giving reasonably good uv coverage. The measured visibilities were replaced by Gaussian distributed noise and dirty images and beams were derived. The RMS variations in the dirty images were measured to test the effects of the weighting and the central facet beam was used to evaluate the sidelobes. Table I gives the results of the beam and RMS results of the calibrator data tests. The “area” is given by:

$$\text{area} \ = \ \Sigma \ |beam_{\text{radius}}| \ \text{radius}^2$$

where $\text{beam}_{\text{radius}}$ is the azimuthally averaged beam value at radius radius and is a measure of the effect of the sidelobes.

The 1-D rendition of the synthesized beams for the Briggs Robust=0 (“optimal”) tests are given in Figure 3 and for the Robust=-0.5 (more “uniform”) tests in Figures 4 and 5.

B. Target Beam

The target field, at declination, 80° S, was observed for the majority of the 12 hour session. Based on the results of the calibrator beam tests, only Robust=-0.5 was used on the target data-set. Beams for a variety of inner tapers were computed and evaluated and are summarized in Table II and Figures 7 and 8.

C. Imaging tests

The target data-set was imaged using a number of inner tapers to evaluate the effect on the image quality. The data were imaged to a radius of 1.5° with outlying fields from the SUMMS catalog using Obit/MFImage; final images are

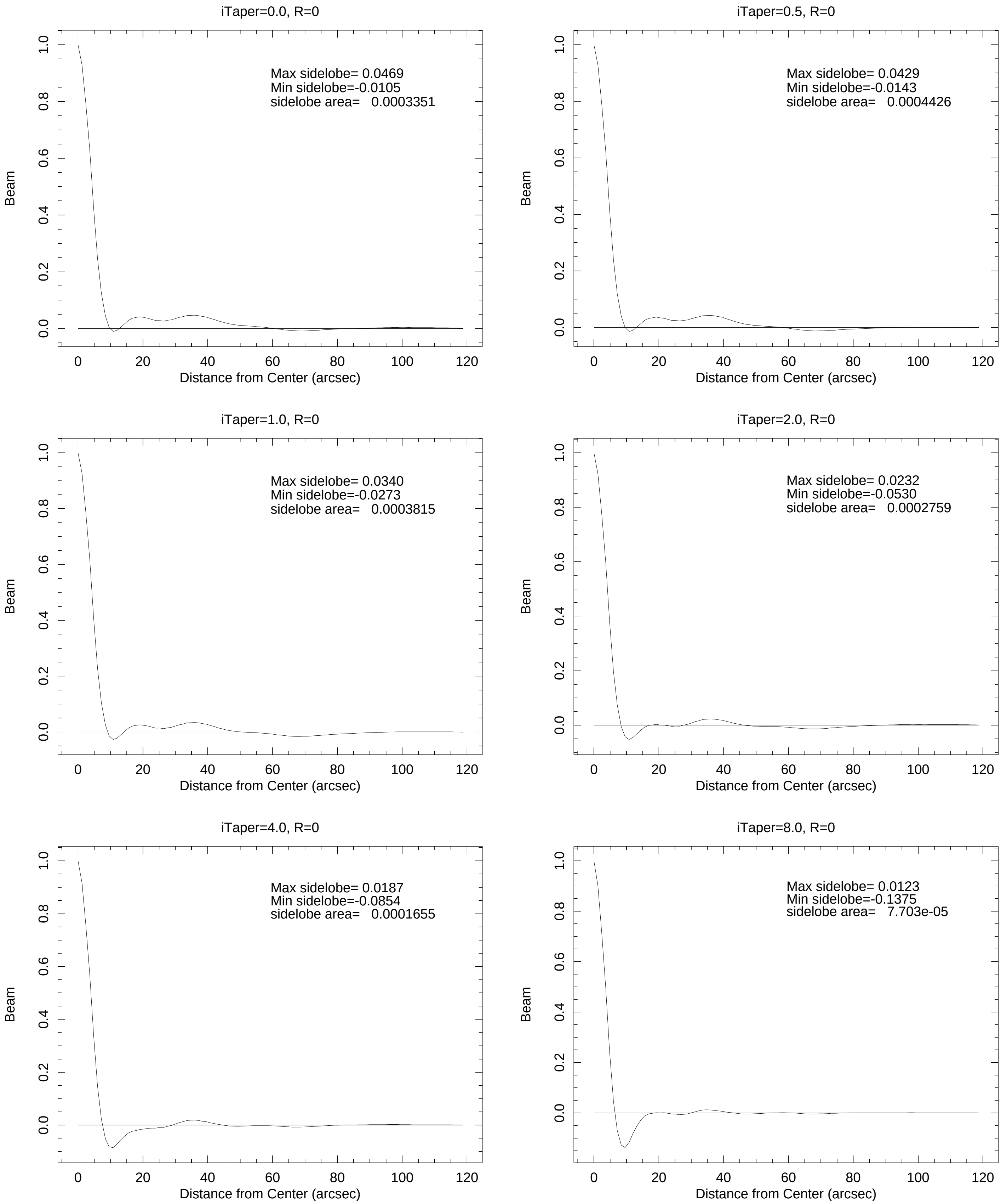

Fig. 3. Azimuthally averaged calibrator beams with Robust=0 and various inner tapers.

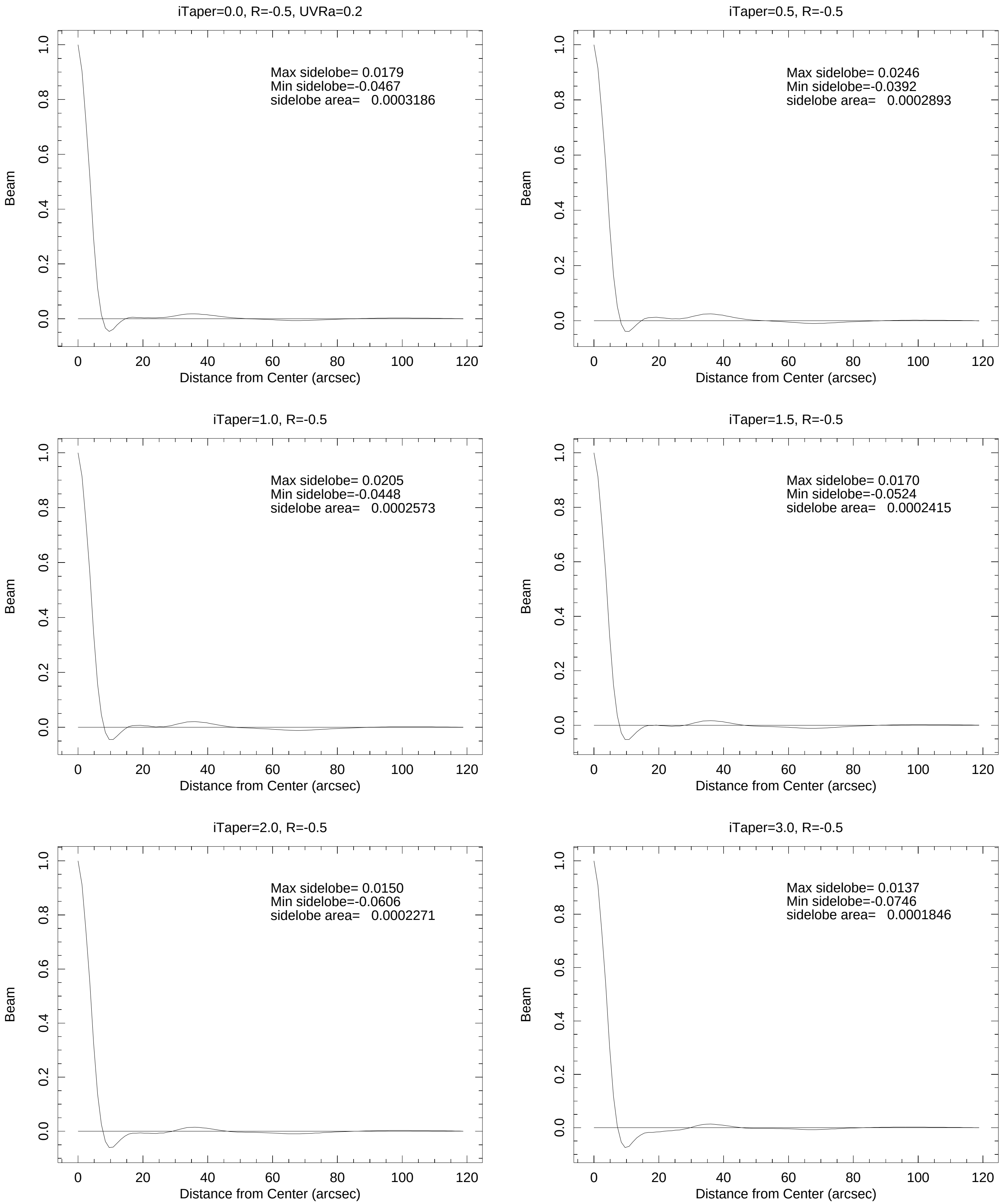

Fig. 4. Azimuthally averaged calibrator beams with Robust=-0.5 and various inner tapers.

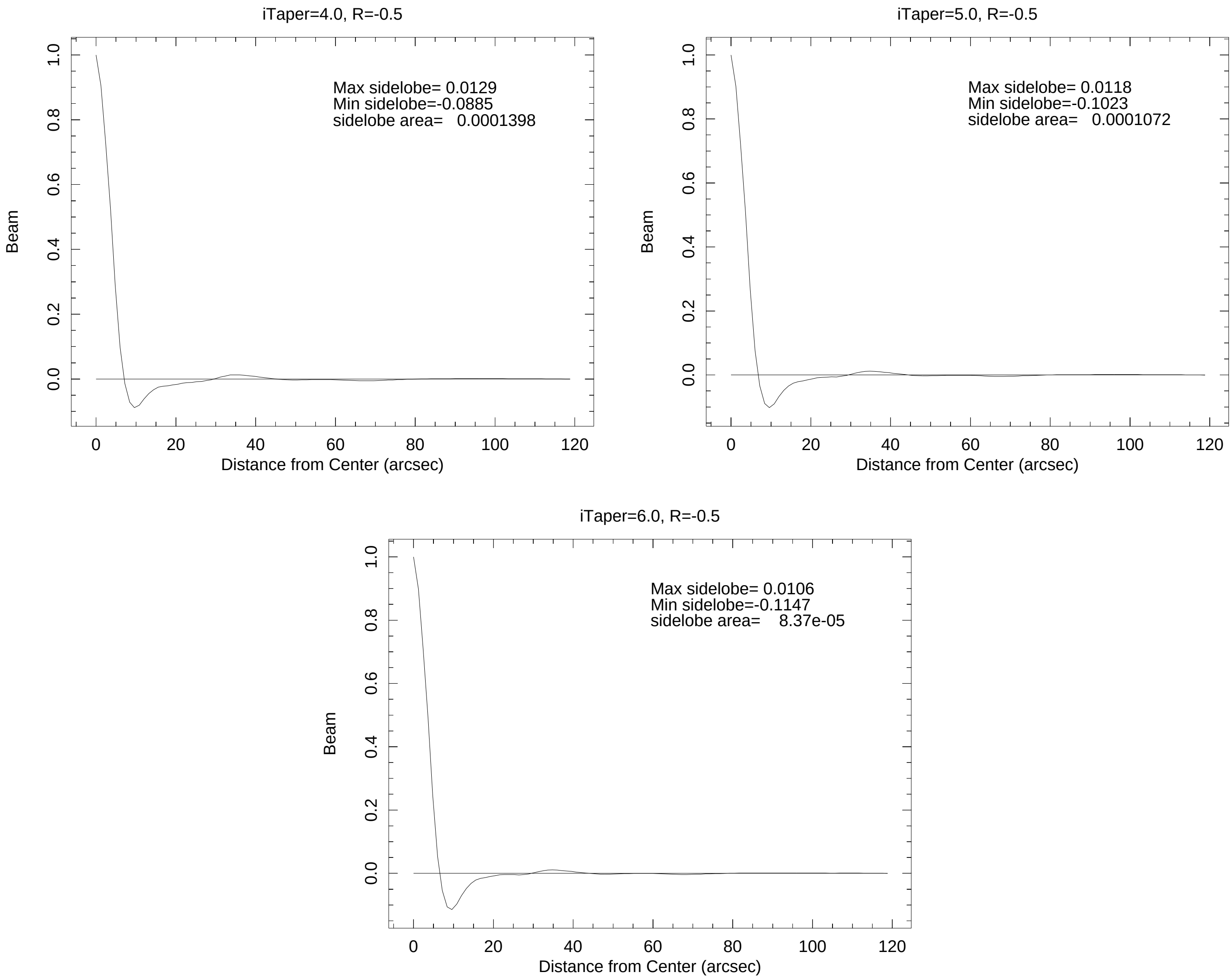

Fig. 5. Azimuthally averaged calibrator beams with Robust=-0.5 Continued.

8970×8970 1.2″ pixels. CLEANing used 100,000 components reaching $\approx 20\mu$Jy/beam. Two iterations of phase only self calibration were applied to the data prior to imaging. Imaging statistics are given in Table III. This table also gives the integrated flux density ("Int") for one of the larger and stronger sources in the field. The distribution of pixel values seems well behaved as is seen in Figure 6.

D. Spatial Filtering

Table II includes a column "fringe" giving the fringe spacing at which the inner taper begins to become important and size scales larger than this will be at least partially filtered out. Most of the sources in the target field are smaller than the synthesized beam but there are several resolved sources. The region containing one of the larger and stronger source is shown in Figure 9. Table III gives the integrated flux density of this source as determined by Obit/imstat The more aggressive inner tapers (higher values) clearly remove extended emission and introduce negative bowls around the source.

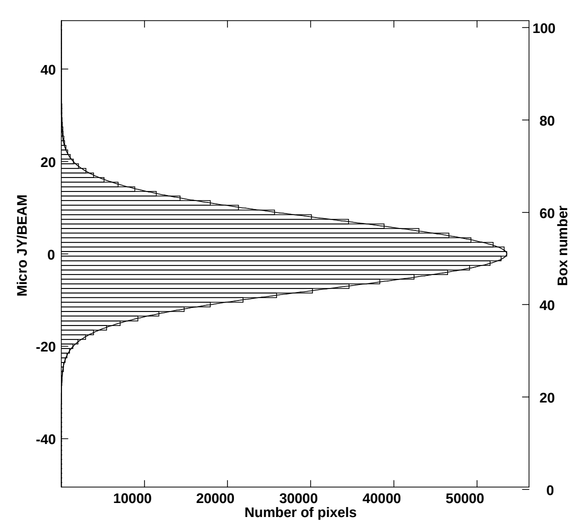

Fig. 6. Histogram of pixel values near edge of image. Curve is fitted Gaussian, $\sigma = 7.44$ μJy/beam.

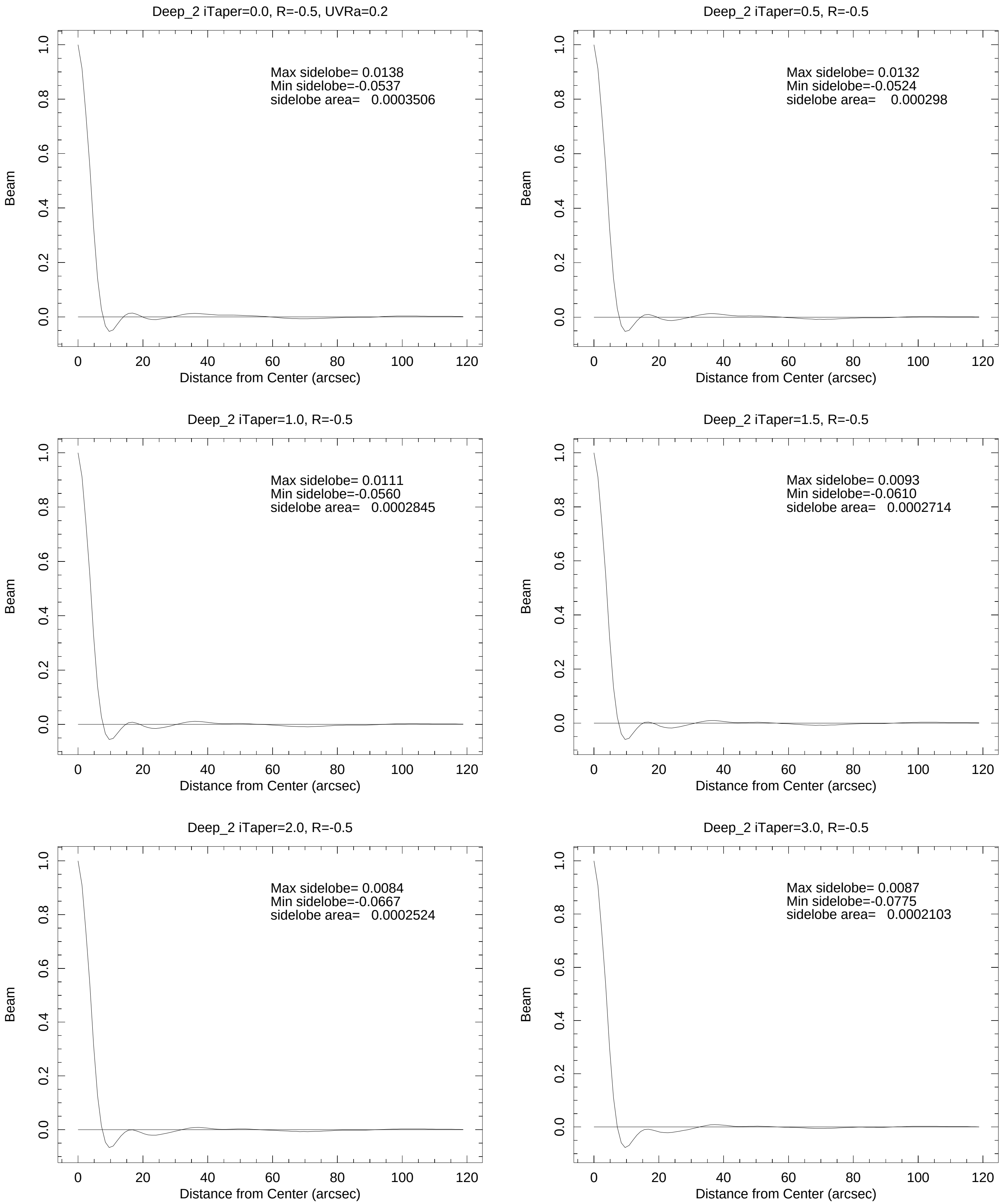

Fig. 7. Azimuthally averaged beams on target field with Robust=-0.5 and various inner tapers.

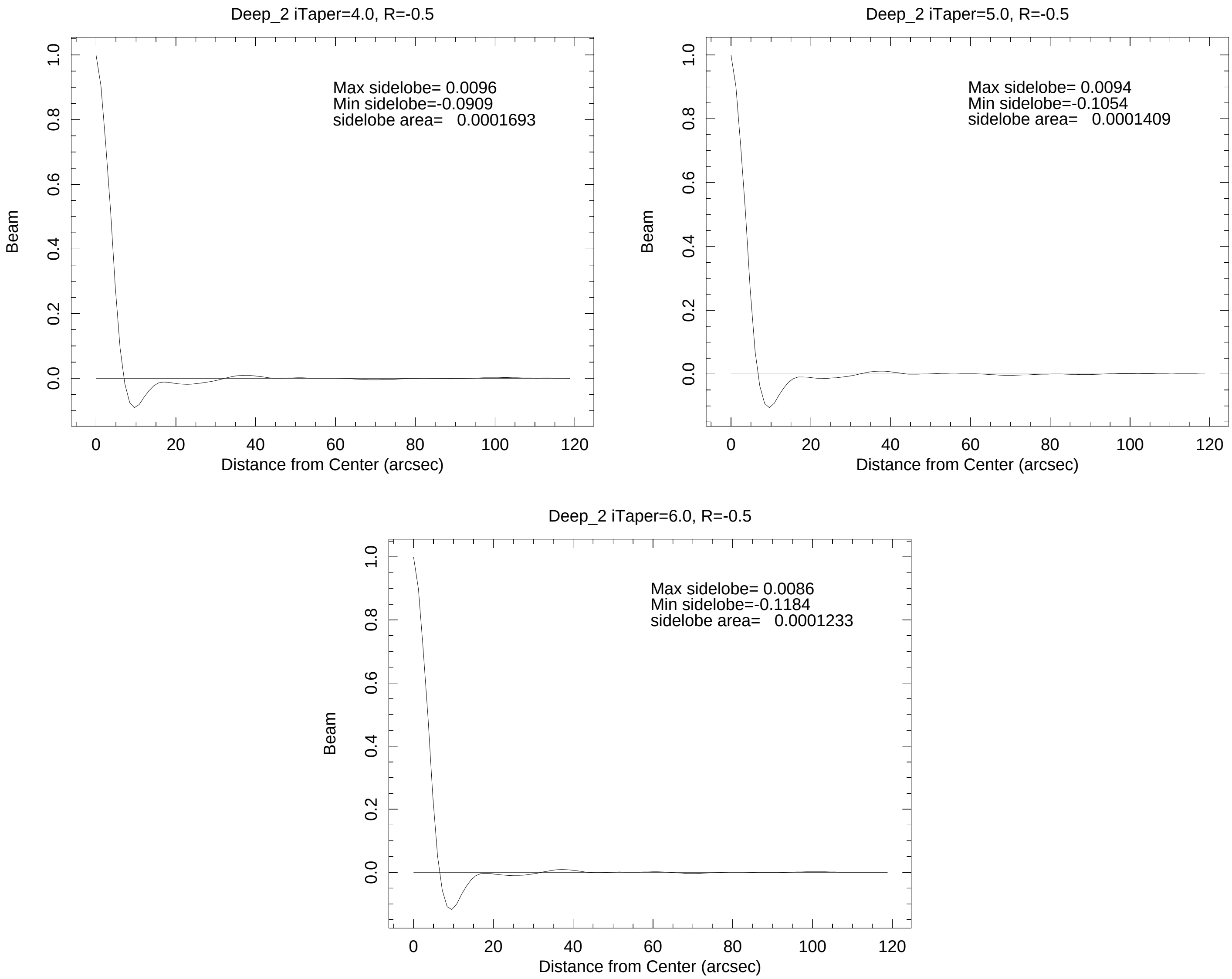

Fig. 8. Azimuthally averaged beams on target field with Robust=-0.5 continued.

E. Confusion

The “noise” in the center of the derived images is the combination of a number of components, 1) thermal noise, 2) artifacts due to limited dynamic range scattering power from sources and 3) “confusion” from the sources which are too weak and blended to detect individually. These components are presumed to be independent so their variances will add:

$$\sigma_{center} = \sqrt{\sigma^2_{thermal} + \sigma^2_{dynamic\_range} + \sigma^2_{confusion}}$$

The expected confusion is on the order of 2.3 μJy/beam based on a scaling of an EVLA measurement at 3 GHz with an $8''$ synthesized beam [2]. The resolutions derived in these tests are a bit smaller than $8''$ so the expected level of confusion will be less. Near the edge of wide area images where the antenna gain is small, only the thermal component of the noise should be present. Comparing the off–source fluctuations near the edge of the image with those near the center should allow separating the thermal from the other components.

Thus, confusion plus “dynamic range” noise can be derived. Table III gives the off–source RMS near the center and near the edge for the imaging tests as well as the quadratic difference. These differences will be the quadratic sum of the dynamic range component and the confusion and are at least twice the expected confusion level, so dynamic range limited.

VII. DISCUSSION

Limitations to dynamic range can come from a number of effects; calibration and pointing errors can cause the true sidelobe pattern to be different from that used in the deconvolution resulting in incorrect subtraction of the source response especially at the locations of major sidelobes. Another limitation on dynamic range is the uv coverage. With the small antennas used by MeerKAT, large areas of the sky are imaged including a very large number of sources; a cataloging of the image gives over 3000 Gaussian components brighter than 50 μJy. Limited uv coverage may contain less information that needed to accurately describe the sources in the field, effectively

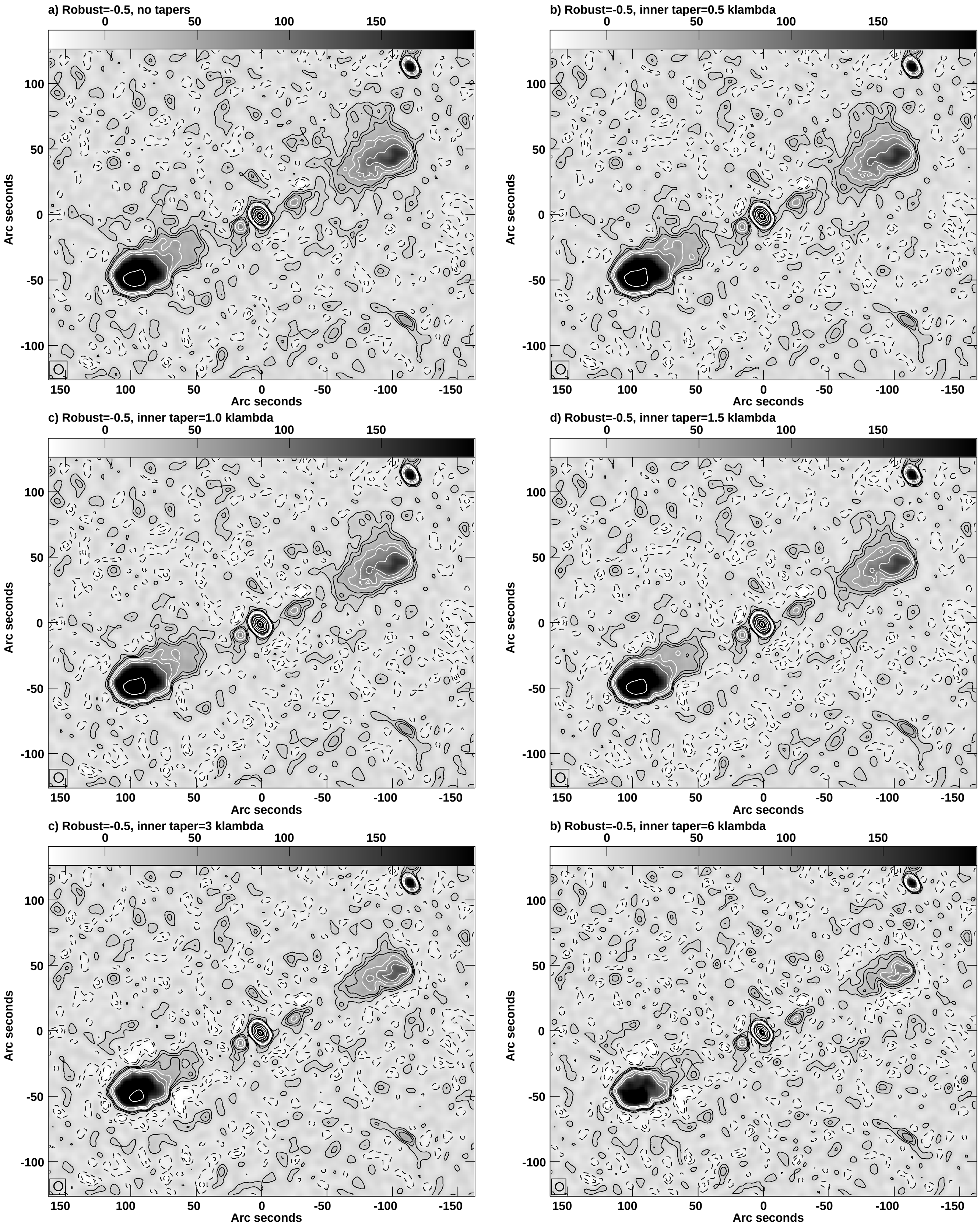

Fig. 9. Image of an FR II source in the target field with various inner tapers and Robust =-0.5. a) no taper, b) taper = 0.5 kλ., c) taper = 1.0 kλ, d) taper = 1.5 kλ., e) taper = 3.0 kλ, f) taper = 6.0 kλ. Images are shown in reversed gray-scale with a scale bar at the top labeled in μJy/beam. Contours are over plotted at -2, -1, 1, 2, 3, 5, 7, 10, 30, 50, 70 and 100 times 10 μJy/beam. Aggressive inner tapers can remove extended emission and leave negative bowls. See Table III for the integrated flux densities in these images.

TABLE I
CALIBRATOR TESTS

iTap kλ	R	θ $''$	RMS	max SL %	min SL %	area
0 [1]	0.0	8.41	3.05	4.69	-1.05	0.0003351
0.5	0.0	8.32	3.06	4.29	-1.43	0.0004426
1.0	0.0	8.11	3.06	3.40	-2.72	0.0003814
2.0	0.0	7.70	2.97	2.32	-5.30	0.0002759
4.0	0.0	7.13	2.92	1.87	-8.54	0.0001655
8.0	0.0	6.26	2.90	1.23	-13.75	0.0000770
0 [1]	-0.5	6.89	2.80	1.79	-4.67	0.0003186
0.5	-0.5	7.42	2.80	2.46	-3.93	0.0002893
1.0	-0.5	7.33	2.81	2.05	-4.48	0.0002573
1.5	-0.5	7.22	2.83	1.70	-5.23	0.0002415
2.0	-0.5	7.11	2.83	1.50	-6.06	0.0002271
3.0	-0.5	6.90	2.85	1.37	-7.47	0.0001846
4.0	-0.5	6.70	2.85	1.30	-8.85	0.0001398
5.0	-0.5	6.50	2.85	1.18	-10.2	0.0001072
6.0	-0.5	6.31	2.86	1.06	-11.5	0.0000837

[1] Used uv range 0.2 to 1000000
Notes: Column “iTap” is the inner taper used; “R” is the Briggs robust factor, “θ” is the synthesized beam FWHM, “RMS” is the RMS of the image in arbitrary units, “max SL” is the maximum sidelobe level, “min SL” is the minimum sidelobe level and “area” is a measure of the area covered by sidelobes.

TABLE II
TARGET TESTS

iTap kλ	fringe $''$	R	θ” $''$	max SL %	min SL %	area
0.0 [1]	1030	-0.5	7.16	1.38	-5.38	0.0003505
0.5	420	-0.5	7.17	1.32	-5.24	0.0002980
1.0	206	-0.5	7.13	1.11	-5.60	0.0002845
1.5	137	-0.5	7.06	0.93	-6.10	0.0002714
2.0	103	-0.5	6.98	0.84	-6.67	0.0002524
3.0	68	-0.5	6.82	0.87	-7.75	0.0002103
4.0	51	-0.5	6.66	0.96	-9.01	0.0001693
5.0	41	-0.5	6.48	0.94	-10.0	0.0001409
6.0	34	-0.5	6.29	0.86	-11.8	0.0001233

[1] Used uv range 0.2 to 1000000
Notes: Column “iTap” is the inner taper used; “fringe” is the fringe spacing corresponding to the 70% weight, “R” is the Briggs robust factor, “θ” is the synthesized beam size, “max SL” is the maximum sidelobe level, “min SL” is the minimum sidelobe level and “area” is a measure of the area covered by sidelobes.

TABLE III
IMAGING TESTS

iTap kλ	θ $''$	Σ Jy	cent. σ μJy/bm	out. σ μJy/bm	σ_{c+DR} μJy/bm	Int mJy
0.0 [1]	6.89	1.0569	9.09	7.41	5.3	10.03
0.5	7.17	1.0592	9.20	7.43	5.4	9.26
1.0	7.13	1.0615	9.12	7.43	5.3	8.36
1.5	7.07	1.0576	9.12	7.43	5.3	7.58
3.0	6.90	1.0491	9.02	7.41	5.1	6.62
6.0	6.31	1.0448	8.88	7.37	5.0	5.01

[1] Used uv range 0.2 to 1000000
Notes: Column “Σ” is the total CLEAN flux density, “θ” is the psf resolution, “cent. σ” is the off source RMS in the central 1000×1000 pixels (full antenna gain), “out. σ” is the off source RMS in 1000×1000 pixels at the edge of the image (very low antenna gain), σ_{c+DR} is the quadratic difference, i.e. the confusion plus dynamic range noise, and “Int” is the integrated flux density of a large FR II radio galaxy.

converting some of the flux density into what appears to be noise.

Using a taper on the short baselines does appear to have the desired effect of reducing the further sidelobes at the expense of increasing the depth of the first, negative sidelobe and filtering out extended emission. Interestingly, the “RMS” given in Table I shows almost no dependence on the inner taper used; the synthesized beam size is affected, effectively changing the units (Jy/beam).

While the emission from extended sources can be filtered out on the more extended sources, the total CLEAN flux density given in Table III is a very weak function of the inner taper meaning that the bulk of the emission may be unaffected. Thus, this technique might be used to reduce a portion of the effects limiting dynamic range. The test beams derived using inner tapers show that the technique is effective at reducing the more distant sidelobes and should have significantly reduced the dynamic range “noise” resulting from them. The near independence of σ_{c+DR} on iTap in Table III suggests that the limited uv coverage and very large number of sources may be the dominant effect. When the full MeerKAT compliment of antennas (64) is available, the uv coverage limitation should be much less.

ACKNOWLEDGMENT

I would like to thank the MeerKAT staff especially Tom Mauch, Simon Perkins and Fernando Camilo for assistance and for providing the data used for these tests. And thanks to Jim Condon for discussions on confusioin and dynamic range limitations.

REFERENCES

[1] W. D. Cotton, “Obit: A Development Environment for Astronomical Algorithms,” *PASP*, vol. 120, pp. 439–448, 2008.
[2] J. J. Condon, W. D. Cotton, E. B. Fomalont, K. I. Kellermann, N. Miller, R. A. Perley, D. Scott, T. Vernstrom, and J. V. Wall, “Resolving the Radio Source Background: Deeper Understanding through Confusion,” *ApJ*, vol. 758, p. 23, Oct. 2012.